Iron-Catalyzed Oxidative C—O and C—N Coupling Reactions Using Air as Sole Oxidant**

Alexander Purtsas,[a] Marco Rosenkranz,[b] Evgenia Dmitrieva,[b] Olga Kataeva,[c] and Hans-Joachim Knölker*[a]
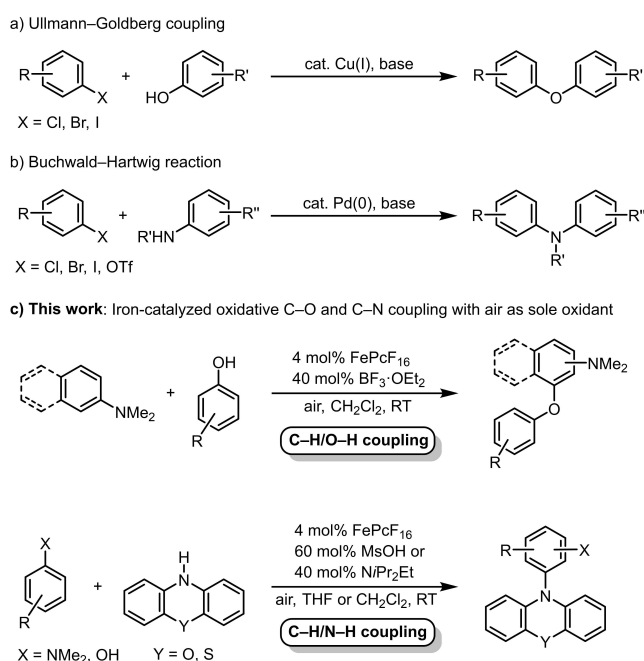
In Memoriam Professor Siegfried Hünig (1921–2021)

Abstract: We describe the oxygenation of tertiary arylamines, and the amination of tertiary arylamines and phenols. The key step of these coupling reactions is an iron-catalyzed oxidative C—O or C—N bond formation which generally provides the corresponding products in high yields and with excellent regioselectivity. The transformations are accomplished using hexadecafluorophthalocyanine–iron(II) (FePcF$_{16}$) as catalyst in the presence of an acid or a base additive and require only ambient air as sole oxidant.

Introduction

The construction of carbon–heteroatom bonds is a crucial transformation for the synthesis of functionalized heterocyclic moieties present in natural products and pharmaceuticals. Transition metal catalysts have been widely applied for these coupling reactions.[1] The best known method to generate C—O bonds for diaryl ethers is the copper-catalyzed Ullmann-Goldberg reaction (Scheme 1a).[2] The palladium-catalyzed Buchwald-Hartwig amination of aryl halides represents a useful tool for C—N bond formation (Scheme 1b).[1c,3] These methods require pre-functionalized substrates, thus limiting their utility from an economic and environmental point of view.[4] Therefore, considerable efforts have been made to achieve a direct C—H bond functionalization by intermolecular oxidative C—O and C—N coupling reactions. A key challenge of the oxidative

a) Ullmann–Goldberg coupling

b) Buchwald–Hartwig reaction

c) **This work**: Iron-catalyzed oxidative C–O and C–N coupling with air as sole oxidant

Scheme 1. Transition metal catalyzed C–O and C–N coupling reactions.

coupling is the fact that C—H bonds are relatively inert and thus, several groups have applied strong oxidants for this process.[5,6] However, these procedures often suffer from low atom-economy, poor selectivity, and harsh reaction conditions. Using green oxidants, the oxidative coupling becomes more attractive.[7] Thus, oxygen from ambient air represents the ideal oxidant due to its natural abundance and environmentally friendly features.[8]

Inspired by green and sustainable chemistry, transition metal-catalyzed oxidative coupling reactions have become a useful and versatile tool for the formation of carbon–heteroatom bonds with air as sole oxidant.[9] Especially copper[9d,10]

[a] A. Purtsas, Prof. Dr. H.-J. Knölker
     Fakultät Chemie
     Technische Universität Dresden
     Bergstraße 66, 01069 Dresden (Germany)
     E-mail: hans-joachim.knoelker@tu-dresden.de
     Homepage: http://www.chm.tu-dresden.de/oc2/

[b] M. Rosenkranz, Dr. E. Dmitrieva
     Center of Spectroelectrochemistry
     Leibniz Institute for Solid State and Materials Research (IFW) Dresden
     Helmholtzstraße 20, 01069 Dresden (Germany)

[c] Dr. O. Kataeva
     A. E. Arbuzov Institute of Organic and Physical Chemistry
     FRC Kazan Scientific Center, Russian Academy of Sciences
     Arbuzov Str. 8, Kazan 420088 (Russia)

Chem. Eur. J. **2022**, 28, e202104292 (1 of 8)

© 2022 The Authors. Chemistry - A European Journal published by Wiley-VCH GmbH

Chemistry–A European Journal

Research Article
doi.org/10.1002/chem.202104292

Chemistry Europe
European Chemical
Societies Publishing

and noble metals[11] have been applied successfully for this purpose.[9f] More recently, the search for inexpensive, less toxic, and thus environmentally benign and sustainable catalysts has come into the focus of interest.[12] Iron compounds are in the center of this development.[13] In this context, iron-based catalysts in combination with stoichiometric amounts of strong oxidants have been extensively studied for oxidative carbon–heteroatom coupling reactions.[14] However due to the hazard of the oxidant, these methods are not a fully sustainable alternative for such conversions. In contrast, iron-catalyzed oxidative carbon–heteroatom coupling reactions using oxygen from ambient air as oxidant represent green synthetic transformations.

Recently, we have developed an oxidative C–C homocoupling of anilines[15,16] and hydroxycarbazoles,[17] as well as an oxidative C–C cross-coupling of tertiary anilines with hydroxyarenes[18] using hexadecafluorophthalocyanine–iron(II) (FePcF$_{16}$, Figure 1)[15,19] as catalyst with air as sole oxidant.[20] The iron-catalyzed reaction of 2-(dimethylamino)naphthalene with 2-naphthol afforded the oxidative C–C cross-coupling product (62% yield) along with a diaryl ether (11% yield) resulting from an oxidative C–O coupling reaction.[18] This previous result prompted us to study the feasibility of novel iron-catalyzed oxidative C–O and C–N coupling reactions. Herein, we report efficient oxygenations and aminations of tertiary arylamines and aminations of phenols in the presence of FePcF$_{16}$ as catalyst and air as sole oxidant at room temperature. The presence of an appropriate additive (Lewis acid, Brønsted acid, or base) is crucial for these mild oxidative carbon–heteroatom bond formations (Scheme 1c).

Results and Discussion

Based on our protocol for the iron-catalyzed oxidative C–C cross-coupling,[18] we investigated the iron-catalyzed oxidative C–O coupling of 2-(dimethylamino)naphthalene (1a) and 4-methoxyphenol (2a) to the diaryl ether 3a in dichloromethane as model reaction (Table 1). No product was formed using catalytic amounts of FePcF$_{16}$ (4 mol%) without additive at room temperature under ambient air (entry 1). Variation of the additives from acetic acid (entry 2) to methanesulfonic acid (entry 3) showed that the stronger Brønsted acid led to the diaryl ether 3a in 25% yield along with the dioxygenated product 4a in 31% yield (entry 3). Lewis acids proved to be
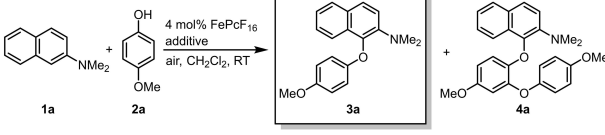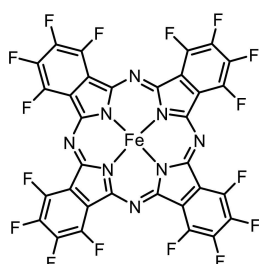
Figure 1. Structure of hexadecafluorophthalocyanine–iron(II) (FePcF$_{16}$).

Table 1. Optimization of the reaction conditions for the iron-catalyzed oxidative C–O coupling of 2-(dimethylamino)naphthalene (1a) with 4-methoxyphenol (2a).[a]
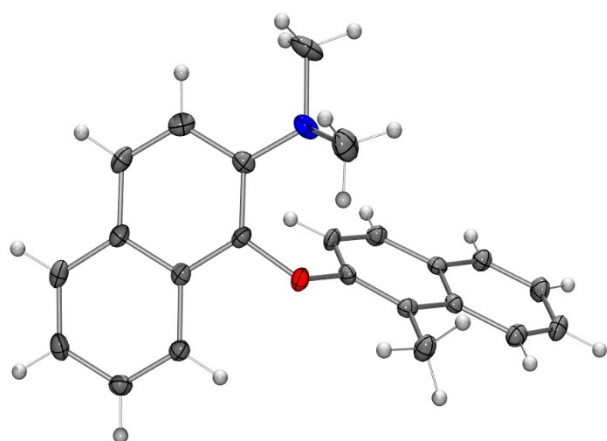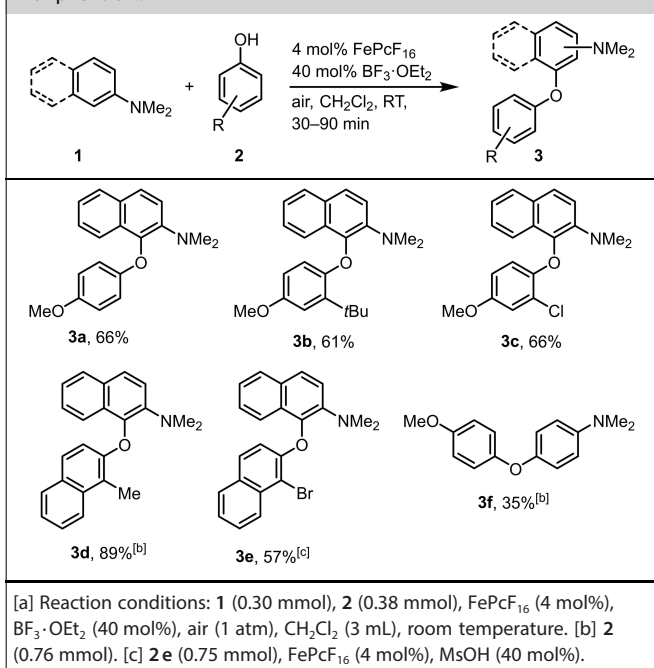
Entry	Additive (mol%)	Time	Yield of 3a [%]	Yield of 4a [%]
1	–	24 h	–	–
2	AcOH (200)	24 h	traces	–
3	MsOH (40)	2 h	25	31
4	B(C$_6$F$_5$)$_3$ (40)	50 min	53	traces
5	BF$_3\cdot$OEt$_2$ (40)	40 min	66	traces
6[b]	BF$_3\cdot$OEt$_2$ (40)	24 h	17	–
7[c]	BF$_3\cdot$OEt$_2$ (40)	3.5 h	36	–

[a] Reaction conditions: 1a (0.30 mmol), 2a (0.38 mmol), FePcF$_{16}$ (4 mol%), air (1 atm), CH$_2$Cl$_2$ (3 mL), room temperature. [b] Solvent: EtOH (3 mL). [c] Reaction at 0 °C. FePcF$_{16}$ = hexadecafluorophthalocyanine–iron(II).

superior providing selectively the diaryl ether 3a as major product (entries 4 and 5). An optimized protocol with 40 mol% of BF$_3\cdot$OEt$_2$ as additive and air as oxidant afforded compound 3a in 66% yield (entry 5). In comparison, the recently reported oxidative coupling of 2-(dimethylamino)naphthalene (1a) with various phenols using a chromium–salen catalyst under aerobic conditions afforded mixtures of C–C and C–O coupling products.[21] Variation of the reaction conditions given in entry 5 of Table 1 gave no further improvement. For example, the very slow reaction in ethanol as solvent afforded 3a in only 17% yield after 24 h (entry 6) and the reaction at 0 °C provided 3a in only 36% yield (entry 7). Moreover, the reaction of entry 5 under an atmosphere of pure oxygen resulted in complete decomposition of the phenol 2a within 12 minutes. Whereas using Fe(acac)$_3$ as catalyst gave no turnover and allowed recovery of the starting materials 1a and 2a.

The iron-catalyzed oxidative C–O coupling of 2-(dimethylamino)naphthalene (1a) with a range of phenols 2a–e using the optimized reaction conditions provided selectively the corresponding diaryl ethers 3a–e (Table 2). Coupling of 1a with 1-methyl-2-naphthol (2d) led to the dinaphthyl ether 3d in 89% yield. The structure of 3d was additionally confirmed by an X-ray analysis (Figure 2).[22] The coupling of 1a with 1-bromo-2-naphthol (2e) required 40 mol% of methanesulfonic acid as additive to afford the dinaphthyl ether 3e in 57% yield. Coupling of N,N-dimethylaniline (1b) with 4-methoxyphenol (2a) provided compound 3f in 35% yield. The reaction with primary and secondary arylamines did not lead to product formation.

The reaction is assumed to proceed via a free-radical coupling mechanism (Scheme 2). Single-electron transfer (SET) oxidation of the phenol by an iron(III) species and subsequent proton loss of the radical cation generate a phenoxy radical which attacks the Lewis acid–Lewis base complex of the tertiary arylamine and boron trifluoride. Cleavage of the boron trifluoride from the resulting cyclohexadienyl radical, oxidation by another SET to a cyclohexadienyl cation, and proton loss
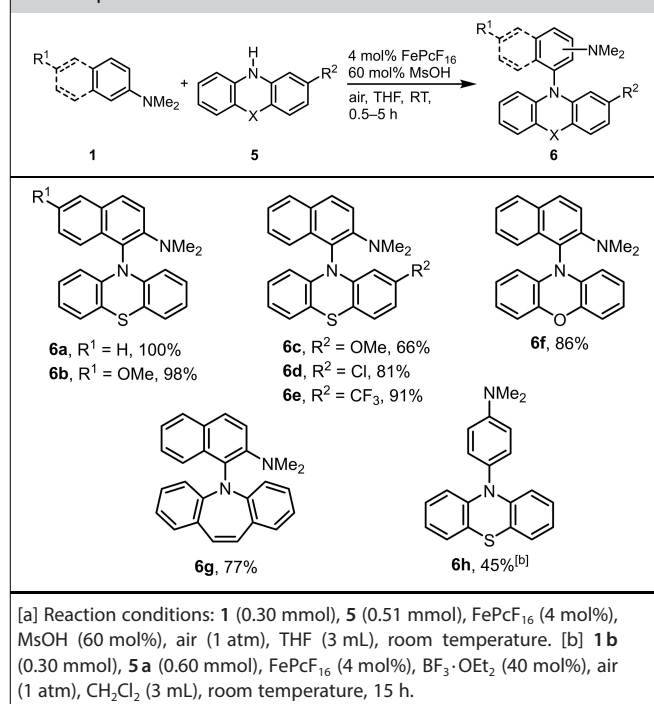
Chemistry–A European Journal

Research Article
doi.org/10.1002/chem.202104292

Chemistry Europe
European Chemical
Societies Publishing

Table 2. Iron-catalyzed oxidative C–O coupling of tertiary arylamines **1** with phenols **2**.[a]

3a, 66% **3b**, 61% **3c**, 66%

3d, 89%[b] **3e**, 57%[c] **3f**, 35%[b]

[a] Reaction conditions: **1** (0.30 mmol), **2** (0.38 mmol), FePcF$_{16}$ (4 mol%), BF$_3$·OEt$_2$ (40 mol%), air (1 atm), CH$_2$Cl$_2$ (3 mL), room temperature. [b] **2** (0.76 mmol). [c] **2e** (0.75 mmol), FePcF$_{16}$ (4 mol%), MsOH (40 mol%).

Figure 2. Molecular structure of the dinaphthyl ether **3d** in the crystal (thermal ellipsoids are shown at the 50% probability level).
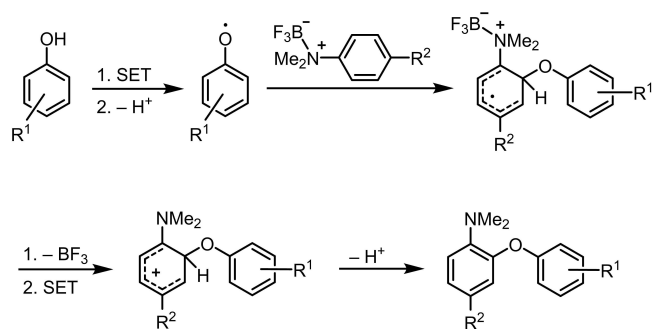
Scheme 2. Proposed mechanism for the iron-catalyzed oxidative C–O coupling of tertiary arylamines with phenols.

afford the diaryl ether. The presence of boron trifluoride as additive appears to be crucial for the success of this oxidative C–O coupling since in the presence of Brønsted acid the C–C cross coupling generally is preferred.[13k,18]

In contrast to the Buchwald-Hartwig amination, the oxidative C–H/N–H coupling represents a more direct and atom-economical method.[23] Phenothiazines, compounds with useful biological[24] and optoelectronic properties,[25] have been applied recently for oxidative C–N coupling reactions by Patureau et al.[26] and other groups.[27] The resulting N-arylated phenothiazines exhibit interesting physical properties.[28]

The iron-catalyzed oxidative C–N coupling reaction of 2-(dimethylamino)naphthalenes **1** with the phenothiazines **5a–d** afforded the corresponding N-arylated products **6a–e** in good to excellent yields (Table 3). An X-ray crystal structure determination of **6a** confirmed the *N*-(1-naphthyl)phenothiazine framework (Figure 3).[29] The optimized reaction conditions for this reaction (4 mol% of FePcF$_{16}$ and 60 mol% of methanesulfonic acid as additive in THF at room temperature under air) closely resemble those previously used for the iron-catalyzed oxidative C–C cross-coupling of tertiary anilines with hydroxyarenes.[18] The blank experiment, reaction of phenothiazine (**5a**) with **1a** in the absence of the catalyst FePcF$_{16}$, afforded compound **6a** in only 11% yield after 3 h. The coupling of 2-(dimethylamino)naphthalene (**1a**) with phenoxazine or dibenzo[*b,f*]azepine provided the corresponding products **6f** and **6g** in high yields, whereas the reaction of *N,N*-dimethylaniline (**1b**) with phenothiazine (**5a**) using BF$_3$·OEt$_2$ (40 mol%) as additive gave a moderate yield for **6h**.

Following the excellent results achieved with phenothiazine (**5a**) as coupling substrate, we have extensively investigated the

Table 3. Iron-catalyzed oxidative C–N coupling of tertiary arylamines **1** with compounds **5**.[a]

6a, R^1 = H, 100% **6c**, R^2 = OMe, 66% **6f**, 86%
6b, R^1 = OMe, 98% **6d**, R^2 = Cl, 81%
  6e, R^2 = CF$_3$, 91%

6g, 77% **6h**, 45%[b]

[a] Reaction conditions: **1** (0.30 mmol), **5** (0.51 mmol), FePcF$_{16}$ (4 mol%), MsOH (60 mol%), air (1 atm), THF (3 mL), room temperature. [b] **1b** (0.30 mmol), **5a** (0.60 mmol), FePcF$_{16}$ (4 mol%), BF$_3$·OEt$_2$ (40 mol%), air (1 atm), CH$_2$Cl$_2$ (3 mL), room temperature, 15 h.
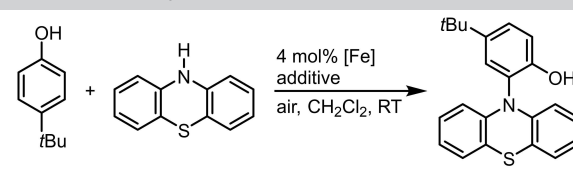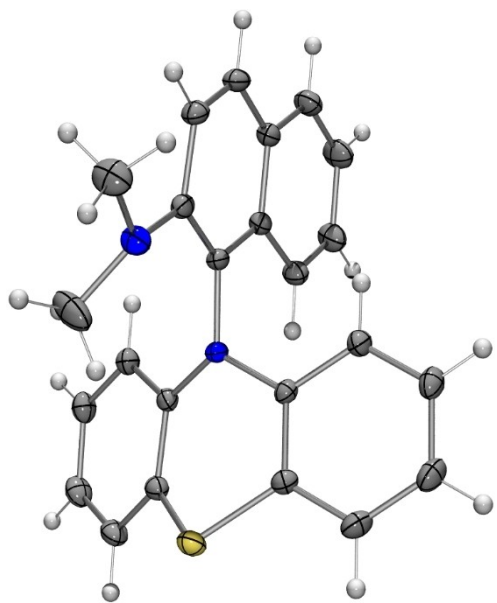
Figure 3. Molecular structure of the *N*-(1-naphthyl)phenothiazine **6a** in the crystal (thermal ellipsoids are shown at the 50% probability level).

Table 4. Optimization of the reaction conditions for the iron-catalyzed oxidative C–N coupling of the phenol **2f** with phenothiazine (**5a**).[a]
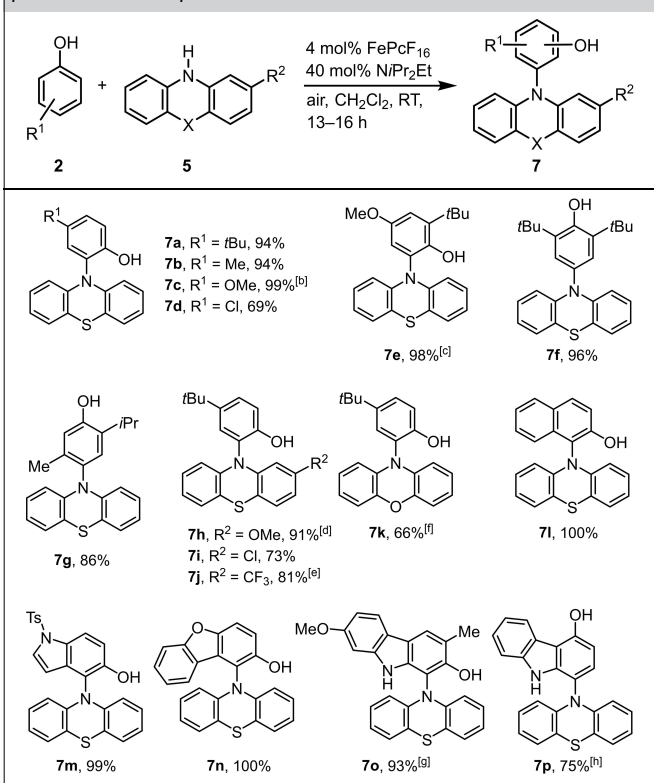

Entry	[Fe] (4 mol%)	Additive (40 mol%)	Time [h]	Yield **7a** [%]
1	FeCl$_2$	–	24	–
2	Fe(acac)$_3$	–	24	–
3	ClFeTPPF$_{20}$	–	24	traces
4	Fe(dbm)$_3$	–	24	15
5	FePc	–	24	18
6	FePcF$_{16}$	–	24	27
7	FePcF$_{16}$	MsOH	2	–
8	FePcF$_{16}$	K$_2$CO$_3$	13	15
9	FePcF$_{16}$	NaOAc	16	20
10	FePcF$_{16}$	NaOtBu	17	48
11	FePcF$_{16}$	DBU	15	15
12	FePcF$_{16}$	DABCO	16	28
13	**FePcF$_{16}$**	**NiPr$_2$Et**	**16**	**94**
14[b]	FePcF$_{16}$	NiPr$_2$Et	14	90
15[c]	μ-oxo(FePcF$_{16}$)$_2$	NiPr$_2$Et	13	96
16[d]	FePcF$_{16}$	NiPr$_2$Et	24	–
17	–	NiPr$_2$Et	24	–
18[e]	FePcF$_{16}$	NiPr$_2$Et	16.5	26
19[f]	FePcF$_{16}$	NiPr$_2$Et	17.5	59
20[g]	FePcF$_{16}$	NiPr$_2$Et	15	51
21	Fe(dbm)$_3$	NiPr$_2$Et	24	20

[a] Reaction conditions: **2f** (0.40 mmol), **5a** (0.80 mmol), air (1 atm), CH$_2$Cl$_2$ (4 mL), room temperature; full conversion of starting material was indicated by TLC analysis. [b] Reaction conditions: **2f** (1.005 g, 6.69 mmol), **5a** (2.68 g, 13.5 mmol), FePcF$_{16}$ (4 mol%, 268 μmol), NiPr$_2$Et (40 mol%, 2.68 mmol), air (1 atm), CH$_2$Cl$_2$ (67 mL), room temperature. [c] **2f** (0.20 mmol), **5a** (0.40 mmol), O(FePcF$_{16}$)$_2$ (2 mol%), air (1 atm), CH$_2$Cl$_2$ (2 mL), room temperature. [d] Reaction under argon. [e] Solvent: EtOAc (4 mL). [f] Solvent: EtOH (4 mL). [g] Solvent: acetone (4 mL). acac = acetylacetonate; DABCO = 1,4-diazabicyclo[2.2.2]octane; dbm = dibenzoyl-methanato; DBU = 1,8-diazabicyclo[5.4.0]undec-7-ene; TPPF$_{20}$ = 5,10,15,20-tetra(pentafluorophenyl)porphyrin.

iron-catalyzed oxidative amination of phenols using the reaction of **5a** with 4-(*tert*-butyl)phenol (**2f**) as model system (Table 4). Various iron compounds as catalysts (4 mol%) and several different additives have been tested for the reaction of **2f** with two equivalents of **5a** at room temperature under ambient air. Simple iron salts as catalysts gave no conversion and 5,10,15,20-tetrakis(pentafluorophenyl)porphyrin–iron(III) chloride led only to traces of the C–N coupling product **7a** (entries 1–3). However, the complex tris(dibenzoylmethanato)iron(III) (Fe[dbm]$_3$),[30] phthalocyanine–iron(II) (FePc), and hexadecafluorophthalocyanine–iron(II) (FePcF$_{16}$) afforded compound **7a** in 15–27% yield (entries 4–6). The high catalytic activity of FePcF$_{16}$ for various oxidative transformations has been widely demonstrated by our group.[15–18,20,31,32] Subsequently, we have screened a range of different additives for the oxidative C–N bond formation using 4 mol% of FePcF$_{16}$ as catalyst (entries 7–13). With methanesulfonic acid as additive (entry 7), complete decomposition of the starting material was observed. Among the different bases tested as additives (entries 8–13), 40 mol% of Hünig's base (*N,N*-diisopropylethylamine) was most beneficial and afforded the C–N cross-coupling product **7a** in 94% yield (entry 13). In this context, it is interesting to note that Hünig's base was also used as additive for the iron-catalyzed oxidative N–N bond formation of diarylamines.[15] These optimized conditions for the iron-catalyzed oxidative C–N coupling could easily be applied to large scale reactions. Thus, a reaction of 300 mg of phenol **2f** provided **7a** in 93% yield and a gram-scale synthesis led to 90% yield of **7a** (entry 14). The first step in FePcF$_{16}$-catalyzed reactions under air is the oxidation of the catalyst to μ-oxobis[(hexadecafluorophthalocyanine)iron(III)] (O[FePcF$_{16}$]$_2$).[32] Thus, using μ-oxo(FePcF$_{16}$)$_2$ as catalyst under otherwise identical conditions gave a similar yield of **7a** (entry 15). In line with our

mechanistic hypothesis of a catalytic [Fe(III)]/[Fe(II)] cycle,[32] the reaction with FePcF$_{16}$ under argon (entry 16) or in the absence of any iron catalyst (entry 17) gave no conversion of the starting materials. In other solvents (ethyl acetate, ethanol, or acetone) the reaction was less efficient than in dichloromethane (entries 18–20). Finally, using Fe(dbm)$_3$ as catalyst in the presence of 40 mol% Hünig's base as additive gave no significant increase of the yield for the coupling product **7a** (compare entries 4 and 21).

Using the optimized conditions (Table 4, entry 13), we investigated the scope of the oxidative C–N coupling reaction of various phenols **2** with phenothiazine (**5a**) (Table 5). While the reaction of anisole with phenothiazine (**5a**) gave no coupling product, simple phenols as substrates provided the *ortho*- or *para*-aminated products **7a–g** in 69–99% yield. It is noteworthy that in the present case the coupling of thymol with phenothiazine (**5a**) led to product **7g** as single regioisomer.[26a] The reaction of 4-(*tert*-butyl)phenol (**2f**) with substituted phenothiazines afforded selectively **7h–j** in 73–91% yield. Shorter reaction times are sufficient for the coupling of **2f**

Chemistry–A European Journal

Research Article
doi.org/10.1002/chem.202104292

Chemistry Europe
European Chemical
Societies Publishing

Table 5. Substrate scope for the iron-catalyzed oxidative C–N coupling of phenols **2** with compounds **5**.[a]

7a, R[1] = tBu, 94%
7b, R[1] = Me, 94%
7c, R[1] = OMe, 99%[b]
7d, R[1] = Cl, 69%

7e, 98%[c]

7f, 96%

7g, 86%

7h, R[2] = OMe, 91%[d]
7i, R[2] = Cl, 73%
7j, R[2] = CF₃, 81%[e]

7k, 66%[f]

7l, 100%

7m, 99%

7n, 100%

7o, 93%[g]

7p, 75%[h]

[a] Reaction conditions: **2** (0.40 mmol), **5** (0.80 mmol), FePcF₁₆ (4 mol%), NiPr₂Et (40 mol%), air (1 atm), CH₂Cl₂ (4 mL), room temperature, 13–16 h. [b] Reaction time: 2.5 h. [c] Reaction time: 5.5 h. [d] **2f** (0.40 mmol), **5b** (1.00 mmol). [e] **2f** (0.40 mmol), **5d** (0.40 mmol). [f] Reaction time: 3 h. [g] **2m** (0.20 mmol), **5a** (0.40 mmol), FePcF₁₆ (4 mol%), NiPr₂Et (40 mol%), air (1 atm), CH₂Cl₂ (2 mL), room temperature, 3.5 h. [h] Reaction time: 6 h.

iron-catalyzed oxidative diamination (Table 6). Compound **8a** was unequivocally confirmed by an X-ray crystal structure determination (Figure 4).[38] Using phenol, *o*-cresol, or *o*-tert-butylphenol as substrates, the same set of reaction conditions led to the diaminated compounds **8b**–**d**. However, the iron-catalyzed oxidative amination of the more electron-rich substrate guaiacol (**2s**) afforded the mono-aminated product **7q** and the diaminated product **8e** only in a 2:1 ratio even with an excess of 4 equivalents of **5a** (Scheme 3). Prolonged reaction times led to no further conversion of **7q** into **8e** but resulted in partial decomposition. The amination at the position *para* to

Table 6. Substrate scope for the twofold iron-catalyzed oxidative C–N coupling of phenols **2** with phenothiazine (**5a**).[a]

8a, 72%

8b, 56%

8c, R = Me, 86%
8d, R = tBu, 89%
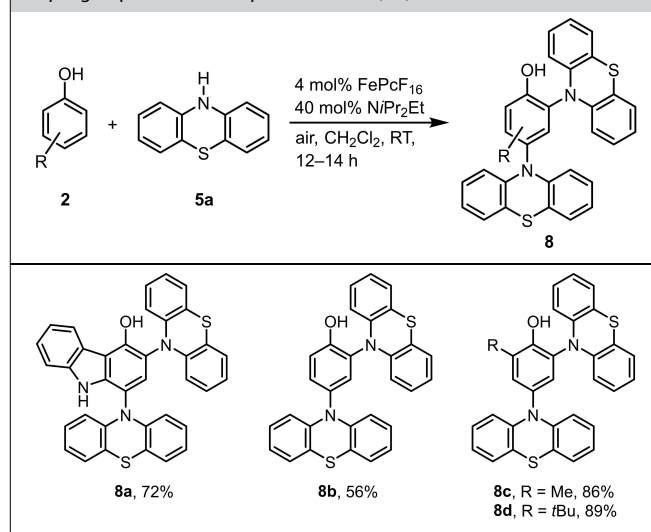
[a] Reaction conditions: **2** (0.40 mmol), **5a** (1.60 mmol), FePcF₁₆ (4 mol%), NiPr₂Et (40 mol%), air (1 atm), CH₂Cl₂ (4 mL), room temperature.
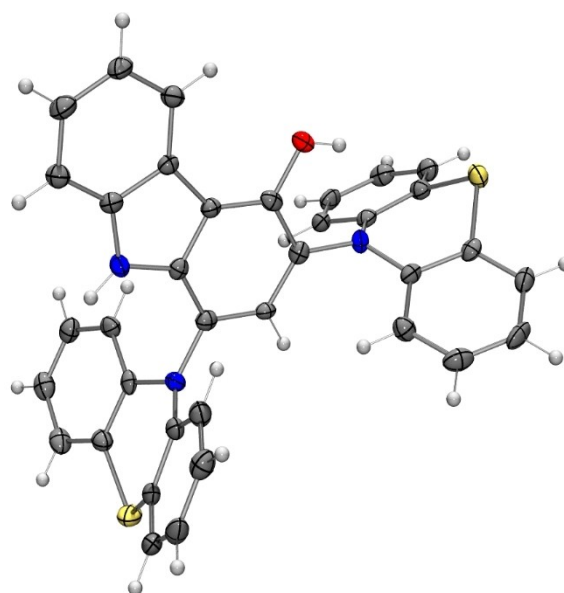
with the more reactive phenoxazine to compound **7k**. Next, we studied the iron-catalyzed oxidative C–N coupling of phenothiazine (**5a**) with polycyclic phenols (2-naphthol, 5-hydroxy-1-tosylindole,[33] 2-hydroxydibenzofuran,[18,34] 2-hydroxy-7-methoxy-3-methylcarbazole,[35] and 4-hydroxycarbazole[36]). These amination reactions provided the corresponding *N*-arylphenothiazines **7l**–**p** regioselectively and in high yields. The regiochemistry of **7p** (amination at C-1 of the carbazole) was confirmed by 2D NMR spectroscopy (COSY, HSQC, HMBC, and NOESY) (see Supporting Information). The synthesis of **7o** and **7p** demonstrates that the present method enables late-stage functionalizations which are difficult to achieve by alternative procedures at the carbazole framework. Carbazoles are an important class of natural products with a broad range of pharmacological activities.[37]
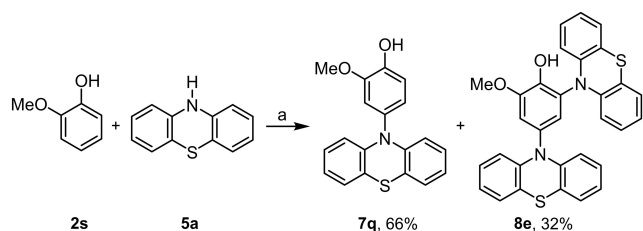
During the synthesis of compound **7p**, we noted that prolonged reaction times lead to formation of a diaminated product. This observation prompted us to study the application of our iron-catalysis to a twofold oxidative C–N bond formation using appropriate substrates. Lei et al. prepared diaminated phenols by electrochemical oxidation.[27c] With an excess of four equivalents of phenothiazine (**5a**), we were able to transform 4-hydroxycarbazole into the corresponding product **8a** by an

Figure 4. Molecular structure of the carbazole **8a** in the crystal (thermal ellipsoids are shown at the 50% probability level; the solvent molecule (CH₂Cl₂) has been omitted for clarity).

Chemistry–A European Journal

Research Article
doi.org/10.1002/chem.202104292

**Chemistry
Europe**
European Chemical
Societies Publishing

Scheme 3. Iron-catalyzed oxidative amination of guaiacol (**2s**) with pheno-thiazine (**5a**). Reaction conditions: a) **2s** (0.40 mmol), **5a** (1.60 mmol), FePcF$_{16}$ (4 mol%), NiPr$_2$Et (40 mol%), air (1 atm), CH$_2$Cl$_2$, room temperature, 14 h.

the hydroxy group in compound **7q** has been assigned based on 2D NMR spectroscopy (COSY, HSQC, HMBC, and NOESY) (see Supporting Information). Xia et al. described an *ortho*-selective coupling between guaiacol (**2s**) and phenothiazine (**5a**).[27a] However, the ^{1}H and ^{13}C NMR data of our compound **7q** are in excellent agreement with those reported by Xia et al. for their corresponding product.[27a] We have additionally confirmed our structural assignment by an X-ray analysis (Figure 5).[39] There-
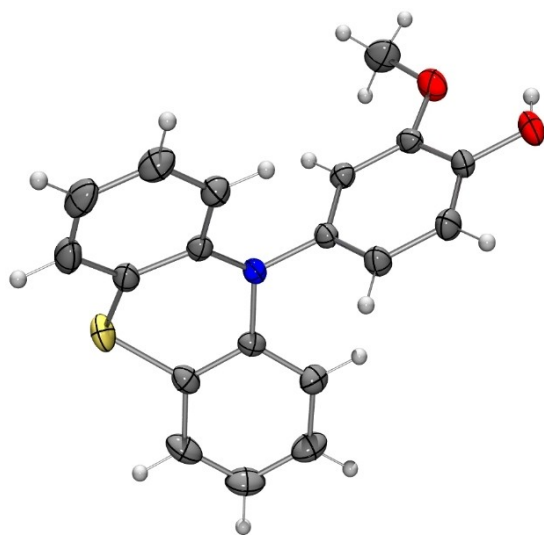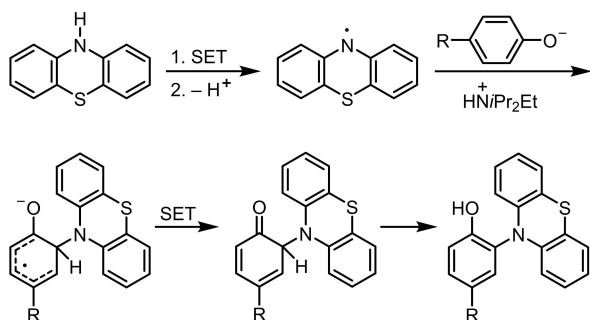

Figure 5. Molecular structure of compound **7q** in the crystal (thermal ellipsoids are shown at the 50% probability level.


Scheme 4. Proposed mechanism for the iron-catalyzed oxidative C–N coupling of phenols with phenothiazine.

fore, the structure of the corresponding product described by Xia et al. has to be revised.

We postulate that the iron-catalyzed amination of phenols with phenothiazine (**5a**) proceeds via a phenothiazine radical intermediate formed by SET to the iron(III) species and subsequent proton loss (Scheme 4). Attack of the phenothiazine radical at the phenolate leads to a cyclohexadienyl radical which is oxidized in another SET to give the final coupling product.[40] Alternatively, the coupling product may be formed by radical recombination of the phenothiazine radical with the phenoxy radical formed as described in Scheme 2.[40e,41] Support for a mechanism via coupling of a phenothiazine free radical derives from a trapping experiment (Scheme 5) and ESR spectroscopy (Figure 6).

Previously, we trapped an aryl radical in the FePcF$_{16}$-catalyzed homocoupling of diarylamines with the free radical scavenger 2,6-di-(*tert*-butyl)-4-methylphenol (BHT).[15] The iron-catalyzed oxidative C–N coupling of phenothiazine (**5a**) with phenols occurs exclusively in the positions *para* and *ortho* to the hydroxy group. Thus, the regiochemical course for this reaction using phenols with *ortho*- and *para*-positions blocked by substituents was in question. The iron-catalyzed oxidative coupling of the *p*-cresol derivatives **9a** (BHT) and **9b** with **5a** under the standard reaction conditions provided the *N*-benzylphenothiazines **10a** and **10b** (Scheme 5). The formation of compounds **10** proceeds via addition of the phenothiazine radical to the corresponding *p*-quinone methides generated by initial oxidation of the *p*-cresols **9**.[42] Moreover, the synthesis of

9a, R = *t*Bu
9b, R = OMe

5a

10a, R = *t*Bu, 46%
10b, R = OMe, 38%
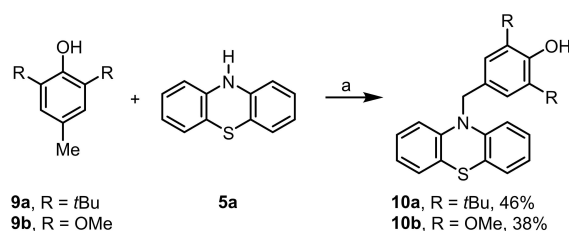
Scheme 5. Iron-catalyzed oxidative C(sp^3)–H/N–H coupling of *para*-cresol derivatives **9** with phenothiazine (**5a**). Reaction conditions: a) **9** (0.40 mmol), **5a** (0.80 mmol), FePcF$_{16}$ (4 mol%), NiPr$_2$Et (40 mol%), air (1 atm), CH$_2$Cl$_2$, room temperature, 15–24 h.
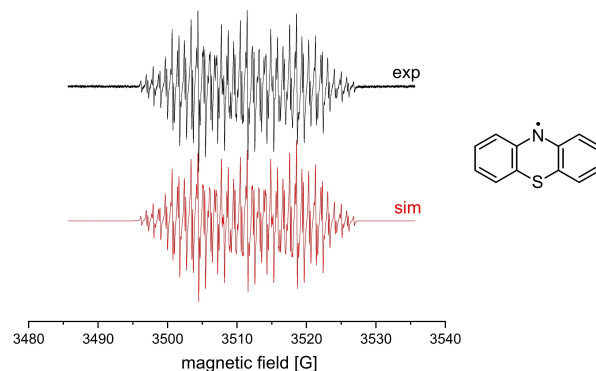

Figure 6. Comparison of the experimental (exp; black) and simulated (sim; red) EPR spectra of the phenothiazine radical at room temperature.

10 indicates that the present methodology can be applied for iron-catalyzed C(sp^3)–H/N–H coupling reactions.

According to the literature, phenothiazine radicals are formed from the parent compounds under oxidative conditions.[26e,27e,43] To get more information on the reaction mechanism of the iron-catalyzed oxidative amination of phenols, we detected the phenothiazine radical generated under the coupling conditions by electron paramagnetic resonance (EPR) spectroscopy. The EPR spectrum of a solution of phenothiazine (**5a**) (0.40 mmol) with FePcF$_{16}$ (2 mol%) and NiPr$_2$Et (20 mol%) in dichloromethane (4 mL) in the presence of air at room temperature after 20 h displays a signal with a hyperfine structure and a g-value of 2.0047 (Figure 6). The experimental and simulated ESR spectra are in nearly perfect agreement. The hyperfine structure is caused by nitrogen ($a(^{14}N) = 7.1$ G) and hydrogen ($a(^1H) = 3.7$, 2.7, 1.0, and 0.8 G) atoms. The observed hyperfine coupling constants are corresponding to those of a neutral N-centered phenothiazine radical.[44]

Conclusion

We have developed a sustainable and efficient iron-catalyzed oxidative C–O and C–N coupling reaction which proceeds at room temperature using hexadecafluorophthalocyanine–iron(II) (FePcF$_{16}$) as catalyst and air as sole oxidant. Utilization of the appropriate additive is crucial for the success of this transformation. Lewis acid is required for the oxygenation of tertiary arylamines. Aminations of tertiary arylamines proceed in the presence of Brønsted acid and those of phenols in the presence of Hünig's base. The structural variety of the resulting coupling products, the excellent selectivity, and the functional group tolerance emphasize the utility of this process. Moreover, the feasibility to achieve oxidative aminations by iron-catalyzed activation of C(sp^3)–H bonds has been indicated. Further studies and applications of the iron-catalyzed oxidative carbon–heteroatom bond formation under aerobic conditions are currently in progress.

Conflict of Interest

The authors declare no conflict of interest.

Data Availability Statement

The data that support the findings of this study are available from the corresponding author upon reasonable request.

[1] a) J. F. Hartwig, *Nature* **2008**, *455*, 314–322; b) *Catalyzed Carbon-Heteroatom Bond Formation* (Ed.: A. K. Yudin), Wiley-VCH, Weinheim, **2010**; c) I. P. Beletskaya, A. V. Cheprakov, *Organometallics* **2012**, *31*, 7753–7808; d) J. Bariwal, E. Van der Eycken, *Chem. Soc. Rev.* **2013**, *42*, 9283–9303; e) V. Ritleng, M. Henrion, M. J. Chetcuti, *ACS Catal.* **2016**, *6*, 890–906; f) B. Seifinoferest, A. Tanbakouchian, B. Larijani, M. Mahdavi, *Asian J. Org. Chem.* **2021**, *10*, 1319–1344.

[2] a) F. Monnier, M. Taillefer, *Angew. Chem. Int. Ed.* **2009**, *48*, 6954–6971; *Angew. Chem.* **2009**, *121*, 7088–7105; b) C. Sambiagio, S. P. Marsden, A. J. Blacker, P. C. McGowan, *Chem. Soc. Rev.* **2014**, *43*, 3525–3550; c) *Copper Catalysis in Organic Synthesis* (Eds.: G. Anilkumar, S. Saranya), Wiley-VCH, Weinheim, **2020**.

[3] a) J. F. Hartwig, in *Handbook of Organopalladium Chemistry for Organic Synthesis*, Vol. 1 (Eds.: E.-i. Negishi, A. de Meijere), Wiley-Interscience, New York, **2002**, 1051–1096; b) P. Ruiz-Castillo, S. L. Buchwald, *Chem. Rev.* **2016**, *116*, 12564–12649; c) R. Dorel, C. P. Grugel, A. M. Haydl, *Angew. Chem. Int. Ed.* **2019**, *58*, 17118–17129; *Angew. Chem.* **2019**, *131*, 17276–17287.

[4] a) R. A. Sheldon, *J. Chem. Technol. Biotechnol.* **1997**, *68*, 381–388; b) D. J. C. Constable, A. D. Curzons, V. L. Cunningham, *Green Chem.* **2002**, *4*, 521–527; c) C.-J. Li, B. M. Trost, *Proc. Natl. Acad. Sci. USA* **2008**, *105*, 13197–13202.

[5] a) *Handbook of C–H Transformations: Applications in Organic Synthesis* (Ed.: G. Dyker), Wiley-VCH, Weinheim, **2005**; b) K. Godula, D. Sames, *Science* **2006**, *312*, 67–72.

[6] a) C. Liu, H. Zhang, W. Shi, A. Lei, *Chem. Rev.* **2011**, *111*, 1780–1824; b) R. Samanta, K. Matcha, A. P. Antonchick, *Eur. J. Org. Chem.* **2013**, 5769–5804; c) X. Zhu, S. Chiba, *Chem. Soc. Rev.* **2016**, *45*, 4504–4523; d) S. Mandal, T. Bera, G. Dubey, J. Saha, J. K. Laha, *ACS Catal.* **2018**, *8*, 5085–5144; e) H. Wang, X. Gao, Z. Lv, T. Abdelilah, A. Lei, *Chem. Rev.* **2019**, *119*, 6769–6787; f) V. Vershinin, D. Pappo, *Org. Lett.* **2020**, *22*, 1941–1946.

[7] a) A. N. Campbell, S. S. Stahl, *Acc. Chem. Res.* **2012**, *45*, 851–863; b) X. Tang, W. Wu, W. Zeng, H. Jiang, *Acc. Chem. Res.* **2018**, *51*, 1092–1105.

[8] C. L. Hill, *Nature* **1999**, *401*, 436–437.

[9] a) S. S. Stahl, *Science* **2005**, *309*, 1824–1826; b) J. Piera, J.-E. Bäckvall, *Angew. Chem. Int. Ed.* **2008**, *47*, 3506–3523; *Angew. Chem.* **2008**, *120*, 3558–3576; c) Z. Shi, C. Zhang, C. Tang, N. Jiao, *Chem. Soc. Rev.* **2012**, *41*, 3381–3430; d) S. E. Allen, R. R. Walvoord, R. Padilla-Salinas, M. C. Kozlowski, *Chem. Rev.* **2013**, *113*, 6234–6458; e) N. Gulzar, B. Schweitzer-Chaput, M. Klussmann, *Catal. Sci. Technol.* **2014**, *4*, 2778–2796; f) *Green Oxidation in Organic Synthesis* (Eds.: N. Jiao, S. S. Stahl), Wiley, Hoboken, NJ, **2019**.

[10] X. Liang, M. Xiong, H. Zhu, K. Shen, Y. Pan, *J. Org. Chem.* **2019**, *84*, 11210–11218.

[11] a) J. Xie, H. Li, Q. Xue, Y. Cheng, C. Zhu, *Adv. Synth. Catal.* **2012**, *354*, 1646–1650; b) Y. Mizuta, K. Yasuda, Y. Obora, *J. Org. Chem.* **2013**, *78*, 6332–6337; c) J. Zhao, C. Mück-Lichtenfeld, A. Studer, *Adv. Synth. Catal.* **2013**, *355*, 1098–1106; d) C. C. Pattillo, I. I. Strambeanu, P. Calleja, N. A. Vermeulen, T. Mizuno, M. C. White, *J. Am. Chem. Soc.* **2016**, *138*, 1265–1272.

[12] a) *Catalysis without Precious Metals* (Ed.: R. M. Bullock), Wiley-VCH, Weinheim, **2010**; b) N. V. Tzouras, I. K. Stamatopoulos, A. T. Papastavrou, A. A. Liori, G. C. Vougioukalakis, *Coord. Chem. Rev.* **2017**, *343*, 25–138; c) *Non-Noble Metal Catalysis: Molecular Approaches and Reactions* (Eds.: R. J. M. Klein Gebbink, M.-E. Moret), Wiley-VCH, Weinheim, **2019**.

[13] a) K. Junge, K. Schröder, M. Beller, *Chem. Commun.* **2011**, *47*, 4849–4859; b) C.-L. Sun, B.-J. Li, Z.-J. Shi, *Chem. Rev.* **2011**, *111*, 1293–1314; c) K. Gopalaiah, *Chem. Rev.* **2013**, *113*, 3248–3296; d) E. Bauer, *Top. Organomet. Chem.* **2015**, *50*, 1–356; e) I. Bauer, H.-J. Knölker, *Chem. Rev.* **2015**, *115*, 3170–3387; f) A. Fürstner, *ACS Cent. Sci.* **2016**, *2*, 778–789; g) R. Shang, L. Ilies, E. Nakamura, *Chem. Rev.* **2017**, *117*, 9086–9139; h) A. Guðmundsson, J.-E. Bäckvall, *Molecules* **2020**, *25*, 1349; i) *Recent Advances in Iron Catalysis* (Ed.: H.-J. Knölker), MDPI, Basel, **2020**; j) J.

Chemistry–A European Journal

Research Article
doi.org/10.1002/chem.202104292

Chemistry
Europe
European Chemical
Societies Publishing

Zhang, S. Wang, Y. Zhang, Z. Feng, *Asian J. Org. Chem.* **2020**, *9*, 1519–1531; k) V. Vershinin, H. Forkosh, M. Ben-Lulu, A. Libman, D. Pappo, *J. Org. Chem.* **2021**, *86*, 79–90; l) S. Rana, J. P. Biswas, S. Paul, A. Paik, D. Maiti, *Chem. Soc. Rev.* **2021**, *50*, 243–472.

[14] a) F. Jia, Z. Li, *Org. Chem. Front.* **2014**, *1*, 194–214; b) X.-H. Yang, R.-J. Song, Y.-X. Xie, J.-H. Li, *ChemCatChem* **2016**, *8*, 2429–2445; c) Y. Ni, X. Wan, H. Zuo, M. A. Bashir, Y. Liu, H. Yu, R.-Z. Liao, G. Wu, F. Zhong, *Org. Chem. Front.* **2021**, *8*, 1490–1495.

[15] R. F. Fritsche, G. Theumer, O. Kataeva, H.-J. Knölker, *Angew. Chem. Int. Ed.* **2017**, *56*, 549–553; *Angew. Chem.* **2017**, *129*, 564–568.

[16] A. Purtsas, S. Stipurin, O. Kataeva, H.-J. Knölker, *Molecules* **2020**, *25*, 1608.

[17] C. Brütting, R. F. Fritsche, S. K. Kutz, C. Börger, A. W. Schmidt, O. Kataeva, H.-J. Knölker, *Chem. Eur. J.* **2018**, *24*, 458–470.

[18] A. Purtsas, O. Kataeva, H.-J. Knölker, *Chem. Eur. J.* **2020**, *26*, 2499–2508.

[19] J. G. Jones, M. V. Twigg, *Inorg. Chem.* **1969**, *8*, 2018–2019.

[20] H.-J. Knölker, *Sitzungsberichte der Sächsischen Akademie der Wissenschaften zu Leipzig – Math.-naturwiss. Klasse*, S. Hirzel, Stuttgart/Leipzig, **2021**, Vol. 133, no. 4, pp. 1–30.

[21] T. J. Paniak, M. C. Kozlowski, *Org. Lett.* **2020**, *22*, 1765–1770.

[22] Crystallographic data for **3d**: $C_{23}H_{21}NO$, $M = 327.41$ g mol^{-1}, crystal size: $0.180 \times 0.226 \times 0.485$ mm^3, monoclinic, space group $P2_1$, $a = 6.1363(6)$, $b = 12.7256(9)$, $c = 11.2193(7)$ Å, $\beta = 98.161(8)°$, $V = 867.22(12)$ Å^3, $Z = 2$, $\rho_{calcd} = 1.254$ g cm^{-3}, $\mu = 0.076$ mm^{-1}, $\lambda = 0.71073$ Å, $T = 100(2)$ K, θ range: 3.59–28.15°, reflections collected: 16916, independent: 4176 ($R_{int} = 0.0746$), 229 parameters. The structure was solved by direct methods and refined by full-matrix least-squares on F^2; final R indices [$I > 2\sigma(I)$]: $R_1 = 0.0509$ and $wR_2 = 0.0946$; maximal residual electron density: 0.188 e Å^{-3}. Deposition Number 2122918 contains the supplementary crystallographic data for this paper. These data are provided free of charge by the joint Cambridge Crystallographic Data Centre and Fachinformationszentrum Karlsruhe Access Structures service.

[23] a) M.-L. Louillat, F. W. Patureau, *Chem. Soc. Rev.* **2014**, *43*, 901–910; b) J. Jiao, K. Murakami, K. Itami, *ACS Catal.* **2016**, *6*, 610–633; c) H. Kim, S. Chang, *ACS Catal.* **2016**, *6*, 2341–2351; d) Y. Park, Y. Kim, S. Chang, *Chem. Rev.* **2017**, *117*, 9247–9301.

[24] M. J. Ohlow, B. Moosmann, *Drug Discov. Today* **2011**, *16*, 119–131.

[25] S. Revoju, A. Matuhina, L. Canil, H. Salonen, A. Hiltunen, A. Abate, P. Vivo, *J. Mater. Chem. C* **2020**, *8*, 15486–15506.

[26] a) M.-L. Louillat-Habermeyer, R. Jin, F. W. Patureau, *Angew. Chem. Int. Ed.* **2015**, *54*, 4102–4104; *Angew. Chem.* **2015**, *127*, 4175–4177; b) R. Jin, F. W. Patureau, *Org. Lett.* **2016**, *18*, 4491–4493; c) P. Y. Vemuri, Y. Wang, F. W. Patureau, *Org. Lett.* **2019**, *21*, 9856–9859; d) F. W. Patureau, *ChemCatChem* **2019**, *11*, 5227–5231; e) C. Cremer, M. Goswami, C. K. Rank, B. de Bruin, F. W. Patureau, *Angew. Chem. Int. Ed.* **2021**, *60*, 6451–6456; *Angew. Chem.* **2021**, *133*, 6525–6530.

[27] a) Y. Zhao, B. Huang, C. Yang, W. Xia, *Org. Lett.* **2016**, *18*, 3326–3329; b) Y. Zhao, B. Huang, C. Yang, B. Li, B. Gou, W. Xia, *ACS Catal.* **2017**, *7*, 2446–2451; c) S. Tang, S. Wang, Y. Liu, H. Cong, A. Lei, *Angew. Chem. Int. Ed.* **2018**, *57*, 4737–4741; *Angew. Chem.* **2018**, *130*, 4827–4831; d) L. Bering, L. D'Ottavio, G. Sirvinskaite, A. P. Antonchick, *Chem. Commun.* **2018**, *54*, 13022–13025; e) K. Liu, S. Tang, T. Wu, S. Wang, M. Zou, H. Cong, A. Lei, *Nat. Commun.* **2019**, *10*, 639; f) P. Zhao, K. Wang, Y. Yue, J. Chao, Y. Ye, Q. Tang, J. Liu, *ChemCatChem* **2020**, *12*, 3207–3211; g) S. Chen, Y.-N. Li, S.-H. Xiang, S. Li, B. Tan, *Chem. Commun.* **2021**, *57*, 8512–8515.

[28] a) M. Chen, S. Deng, Y. Gu, J. Lin, M. J. MacLeod, J. A. Johnson, *J. Am. Chem. Soc.* **2017**, *139*, 2257–2266; b) S. Dadashi-Silab, X. Pan, K. Matyjaszewski, *Chem. Eur. J.* **2017**, *23*, 5972–5977; c) H. Gong, Y. Zhao, X. Shen, J. Lin, M. Chen, *Angew. Chem. Int. Ed.* **2018**, *57*, 333–337; *Angew. Chem.* **2018**, *130*, 339–343; d) Z. Zhou, C. E. Hauke, B. Song, X. Li, P. J. Stang, T. R. Cook, *J. Am. Chem. Soc.* **2019**, *141*, 3717–3722; e) Z. Zhang, X. Fang, Z. Liu, H. Liu, D. Chen, S. He, J. Zheng, B. Yang, W. Qin, X. Zhang, C. Wu, *Angew. Chem. Int. Ed.* **2020**, *59*, 3691–3698; *Angew. Chem.* **2020**, *132*, 3720–3727.

[29] Crystallographic data for **6a**: $C_{24}H_{20}N_2S$, $M = 368.48$ g mol^{-1}, crystal size: $0.332 \times 0.346 \times 0.441$ mm^3, monoclinic, space group $P2_1/n$, $a = 8.7909(3)$, $b = 18.8088(6)$, $c = 11.4079(4)$ Å, $\beta = 99.1274(12)°$, $V = 1862.37(11)$ Å^3, $Z = 4$, $\rho_{calcd} = 1.314$ g cm^{-3}, $\mu = 0.185$ mm^{-1}, $\lambda = 0.71073$ Å, $T = 140(2)$ K, θ range: 2.58–30.52°, reflections collected: 193089, independent: 5680 ($R_{int} = 0.0276$), 246 parameters. The structure was solved by direct

methods and refined by full-matrix least-squares on F^2; final R indices [$I > 2\sigma(I)$]: $R_1 = 0.0336$ and $wR_2 = 0.1031$; maximal residual electron density 0.444 e Å^{-3}. Deposition Number 2122920 contains the supplementary crystallographic data for this paper. These data are provided free of charge by the joint Cambridge Crystallographic Data Centre and Fachinformationszentrum Karlsruhe Access Structures service.

[30] F. Puls, P. Linke, O. Kataeva, H.-J. Knölker, *Angew. Chem. Int. Ed.* **2021**, *60*, 14083–14090; *Angew. Chem.* **2021**, *133*, 14202–14209.

[31] a) F. Puls, H.-J. Knölker, *Angew. Chem. Int. Ed.* **2018**, *57*, 1222–1226; *Angew. Chem.* **2018**, *130*, 1236–1240; b) F. Puls, O. Kataeva, H.-J. Knölker, *Eur. J. Org. Chem.* **2018**, 4272–4276.

[32] F. Puls, F. Seewald, V. Grinenko, H.-H. Klauß, H.-J. Knölker, *Chem. Eur. J.* **2021**, *27*, 16776–16787.

[33] F. Ito, K. Shudo, K. Yamaguchi, *Tetrahedron* **2011**, *67*, 1805–1811.

[34] B. Chiranjeevi, G. Koyyada, S. Prabusreenivasan, V. Kumar, P. Sujitha, C. G. Kumar, B. Sridhar, S. Shaik, M. Chandrasekharam, *RSC Adv.* **2013**, *3*, 16475–16485.

[35] R. Hesse, A. Jäger, A. W. Schmidt, H.-J. Knölker, *Org. Biomol. Chem.* **2014**, *12*, 3866–3876.

[36] C. Brütting, R. Hesse, A. Jäger, O. Kataeva, A. W. Schmidt, H.-J. Knölker, *Chem. Eur. J.* **2016**, *22*, 16897–16911.

[37] a) H.-J. Knölker, K. R. Reddy in *The Alkaloids*, Vol. 65 (Ed.: G. A. Cordell), Academic Press, London, **2008**, pp. 1–430; b) A. W. Schmidt, K. R. Reddy, H.-J. Knölker, *Chem. Rev.* **2012**, *112*, 3193–3328.

[38] Crystallographic data for **8a**: $C_{36}H_{23}N_3OS_2 + CH_2Cl_2$, $M = 662.62$ g mol^{-1}, crystal size: $0.082 \times 0.200 \times 0.937$ mm^3, triclinic, space group $P\bar{1}$, $a = 11.6962(5)$, $b = 12.1077(6)$, $c = 12.4500(6)$ Å, $\alpha = 99.703(4)$, $\beta = 103.383(5)$, $\gamma = 110.795(5)°$, $V = 1541.35(14)$ Å^3, $Z = 2$, $\rho_{calcd} = 1.428$ g cm^{-3}, $\mu = 0.383$ mm^1, $\lambda = 0.71073$ Å, $T = 100(2)$ K, θ range: 1.87–26.99°, reflections collected: 14128, independent: 6500 ($R_{int} = 0.1119$), 414 parameters. The structure was solved by direct methods and refined by full-matrix least-squares on F^2; final R indices [$I > 2\sigma(I)$]: $R_1 = 0.0660$ and $wR_2 = 0.1457$; maximal residual electron density 0.841 e Å^{-3}. Deposition Number 2122922 contains the supplementary crystallographic data for this paper. These data are provided free of charge by the joint Cambridge Crystallographic Data Centre and Fachinformationszentrum Karlsruhe Access Structures service.

[39] Crystallographic data for **7q**: $C_{19}H_{15}NO_2S$, $M = 321.38$ g mol^{-1}, crystal size: $0.120 \times 0.548 \times 0.702$ mm^3, monoclinic, space group $P2_1/n$, $a = 9.024(2)$, $b = 13.929(4)$, $c = 13.159(4)$ Å, $\beta = 108.997(13)°$, $V = 1563.9(8)$ Å^3, $Z = 4$, $\rho_{calcd} = 1.365$ g cm^{-3}, $\mu = 0.216$ mm^{-1}, $\lambda = 0.71073$ Å, $T = 175(2)$ K, θ range: 2.19–28.99°, reflections collected: 51118, independent: 4103 ($R_{int} = 0.0325$), 212 parameters. The structure was solved by direct methods and refined by full-matrix least-squares on F^2; final R indices [$I > 2\sigma(I)$]: $R_1 = 0.0365$ and $wR_2 = 0.0898$; maximal residual electron density 0.289 e Å^{-3}. Deposition Number 2143657 contains the supplementary crystallographic data for this paper. These data are provided free of charge by the joint Cambridge Crystallographic Data Centre and Fachinformationszentrum Karlsruhe Access Structures service.

[40] a) M. Hovorka, J. Günterová, J. Závada, *Tetrahedron Lett.* **1990**, *31*, 413–416; b) M. Hovorka, J. Závada, *Tetrahedron* **1992**, *48*, 9517–9530; c) M. Smrčina, Š. Vyskočil, B. Máca, M. Polášek, T. A. Claxton, A. P. Abbott, P. Kočovský, *J. Org. Chem.* **1994**, *59*, 2156–2163; d) H. Egami, K. Matsumoto, T. Oguma, T. Kunisu, T. Katsuki, *J. Am. Chem. Soc.* **2010**, *132*, 13633–13635; e) I. Fleming, *Molecular Orbitals and Organic Chemical Reactions*, Wiley, Chichester (UK), **2009**, chap. 7 "Radical Reactions".

[41] D. Leifert, A. Studer, *Angew. Chem. Int. Ed.* **2020**, *59*, 74–108; *Angew. Chem.* **2020**, *132*, 74–110.

[42] M. A. R. Raycroft, J.-P. R. Chauvin, M. S. Galliher, K. J. Romero, C. R. J. Stephenson, D. A. Pratt, *Chem. Sci.* **2020**, *11*, 5676–5689.

[43] M. Goswami, A. Konkel, M. Rahimi, M.-L. Louillat-Habermeyer, H. Kelm, R. Jin, B. de Bruin, F. W. Patureau, *Chem. Eur. J.* **2018**, *24*, 11936–11943.

[44] M. F. Chiu, B. C. Gilbert, P. Hanson, *J. Chem. Soc. B* **1970**, 1700–1708.